$LaNi_xFe_{1-x}O_{3-\delta}$ as a Robust Redox Catalyst for CO_2-Splitting and Methane Partial Oxidation

Sherafghan Iftikhar[1], Qiongqiong Jiang[1,2], Yunfei Gao[1], Junchen Liu[1], Haiming Gu[1,3], Luke Neal[1], and Fanxing Li[1*]

[1.]Department of Chemical and Biomolecular Engineering, North Carolina State University, 911 Partners Way, Raleigh, NC 27695-7905, United States.

[2.]Institute of Engineering Thermophysics, Chinese Academy of Sciences, Beijing 100190 China.

[3.]School of Energy and Power Engineering, Nanjing Institute of Technology, Nanjing 211167, China

* E-mail: fli5@ncsu.edu

TOC Graphic

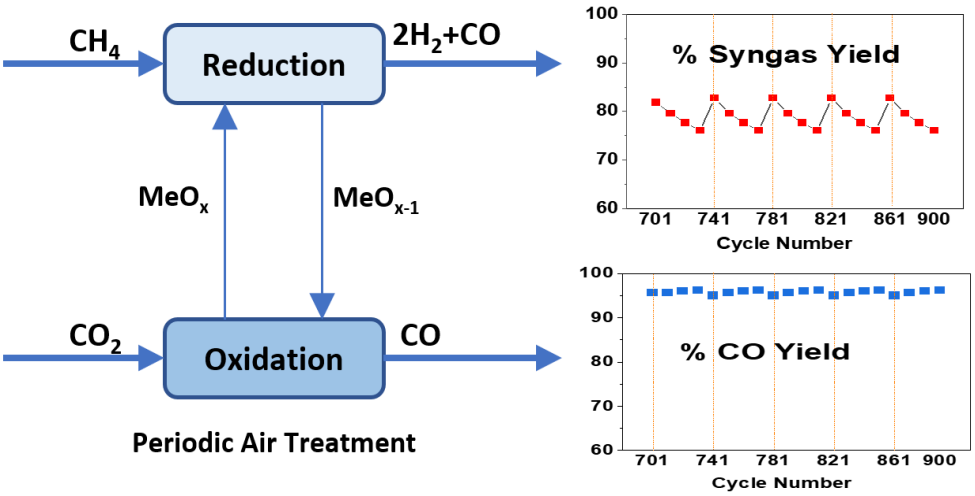

Abstract

The current study reports $LaNi_{0.5}Fe_{0.5}O_{3-\delta}$ as a robust redox catalyst for CO_2-Splitting and methane partial oxidation at relatively low temperatures (~700 °C) in the context of a hybrid redox process (HRP). Specifically, perovskite structured $LaNi_xFe_{1-x}O_{3-\delta}$ (LNF) with nine different compositions (x = 0.05 – 0.5) were prepared and investigated. Among the samples evaluated, $LaNi_{0.4}Fe_{0.6}O_{3-\delta}$ and $LaNi_{0.5}Fe_{0.5}O_{3-\delta}$ showed superior redox performance, with ~90% CO_2 and methane conversions and >90% syngas selectivity. The standalone LNFs also demonstrated performance comparable to that of LNF promoted by mixed conductive $Ce_{0.85}Gd_{0.1}Cu_{0.05}O_{2-\delta}$ (CGCO). Long-term testing of $LaNi_{0.5}Fe_{0.5}O_{3-\delta}$ indicated that the redox catalyst gradually loses its activity over repeated redox cycles, amounting to approximately 0.02% activity loss each cycle, averaged over 500 cycles. This gradual deactivation was found to be reversible by deep oxidation with air. Further characterizations indicated that the loss of activity was resulted from a slow accumulation of iron carbide (Fe_3C and Fe_5C_2) phases, which cannot be effectively removed during the CO_2 splitting step. Reoxidation with air removed the carbide phases, increased the availability of Fe for the redox reactions via solid state reactions with La_2O_3, and decreased the average crystallite size of La_2O_3. Reactivating the redox catalyst periodically, e.g. once every 40 cycles, was shown to be highly effective, as confirmed by operating the redox catalyst over 900 cumulative cycles while maintaining satisfactory redox performance.

Key words: Chemical looping, CO_2-splitting, methane partial oxidation, perovskite, redox catalyst

1. Introduction

Carbon dioxide is a major contributor to global climate change.[1] 43 billion metric tons of CO_2 was emitted in 2019, more than twice the target value of 20 billion metric tons/year for 2040.[2] Most of the emitted CO_2 is resulted from combustion of fossils fuels as energy sources. Specifically, contribution from the industrial sector in GHG emissions was near 23% in United States (2019).[3] Although extensive research has been carried out to develop alternative, environment friendly energy sources, fossil fuels are still expected to play an important role, with an estimated annual increase of 1.4% on average through 2035.[4] Therefore, efficient and economically viable carbon dioxide capture, storage, and utilization technologies are highly desirable.[5–8] In terms of CO_2 utilization, converting CO_2 to CO, an important building block in the chemical industry, offers the opportunity to produce a variety of value-added products.[9] However, breaking the C=O bond in CO_2 is highly energy intensive.[10] To utilize CO_2, electrochemical and photochemical methods have been considered recently but they face different challenges such as low CO_2 conversion, limited energetic efficiency, slow electron transfer, and/or low photon efficiencies.[11] Thermochemical conversion of CO_2 to CO is another alternative that utilizes an oxygen carrier, also known as a redox catalyst, in which the oxygen carrier is first reduced by thermal decomposition and followed by CO_2 splitting to replenish the lattice oxygen released in the thermal decomposition step.[12–15] Although the thermochemical approach is attractive, high operating temperature (>1100 ^{o}C) and limited CO_2 conversion remains as key challenges.[16,17] Methane has this ability to reduce the metal oxide at relatively low temperatures[18–20] which can be advantageous for CO_2 splitting. Once such example is the dry reforming of methane which offers an opportunity to utilize CO_2 by producing syngas with a hydrogen to CO ratio of around one.[21–25] However, the low H_2/CO ratio limits its potential applications unless a fraction of CO is separated from the syngas stream. To address this challenge, we proposed an open-loop Hybrid Redox Process (HRP) concept for thermochemical reduction of CO_2 and methane partial oxidation.[26,27] HRP works in two steps as shown in the Figure 1. In the first step, a redox catalyst reacts with methane to yield synthesis gas (R1) with a H_2: CO ratio near 2:1, which is suitable for methanol and Fischer-Tropsch synthesis.[28] The reduced redox catalyst then reacts with an oxidizing agent such as CO_2 to yield CO (R2). The system further offers the flexibility for downstream carbonylation chemistry, for

example, to produce acetic acid using methanol and CO products without the needs for syngas separation.[29] Compared to conventional thermochemical CO_2 splitting approaches, the use of methane as the reducing agent in HRP can significantly lower the operating temperature for CO_2-splitting.[26]

$$CO_2 + MeO_{x-1} = MeO_x + CO \qquad (R1)$$

$$CH_4 + MeO_x = MeO_{x-1} + CO + 2H_2 \qquad (R2)$$

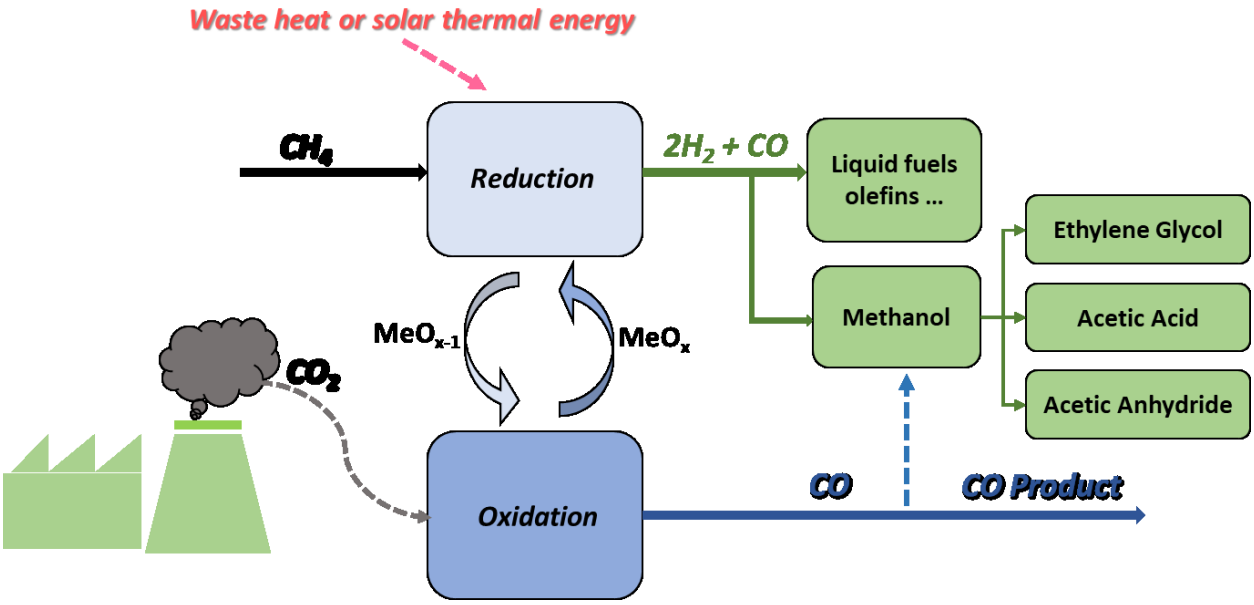

Figure 1. *A simplified schematic of the hybrid redox process.*

Besides the ability to effectively split CO_2, an ideal redox catalyst for HRP should have high CO selectivity in the methane partial oxidation (POx) step and avoid the side reactions such as complete combustion and methane decomposition[30]. In addition, the redox catalyst should be stable over repeated redox cycles. Previous studies have shown that the oxides and mixed oxides of iron, cobalt, and/or nickel with various supports are potentially suitable candidates for

methane POx and thermochemical CO_2-splitting.[7,20,31,32] For example, nanostructured Fe@SiO_2 and Fe–BHA (barium hexa-aluminate) were investigated by Veser et al.[21] in a chemical looping dry reforming (CLDR) scheme within a temperature range of 500-800 ^oC. Fe-supported on BHA showed better redox kinetics and stability compared to Fe@SiO_2 at 800 ^oC. The formation of silicates and partial distortion of the core-shell structure, caused by the poor hydrothermal stability of SiO_2 at the high temperatures, was found to be the main reason for the catalyst deactivation in the nanostructured Fe@SiO_2. In another study, the redox performance of iron-based oxygen carriers were enhanced by synthesising iron-nickel mixed oxides and the results indicated high methane and CO_2 conversions, both above 90% for CLDR at near 1000^oC. The product selectivities were approximately 95%[33]. Ceria-based oxides have also been investigated as the oxygen carriers, reporting near 95% CO_2 conversion in CLDR at 800^oC. However, syngas yield was limited (~38%) due to the low selectivity.[34,35] Recent experimental and density functional theory (DFT) studies have also shown that perovskites, with a general formula $ABO_{3-\delta}$, are suitable for redox reactions.[36–38] For example, Michalsky et al.[39] synthesized $La_{0.6}Sr_{0.4}Co_{0.2}Fe0.8O_{3-\delta}$ (LSCF) to carry out the dry reforming of methane (DRM) in a membrane reactor and found that the results were promising in a temperature range of 840 -1030 ^oC. Zhang et al.[40] reported nanocomposites of $Sr_3Fe_2O_{7-\delta}$ and (Ca/Mn)O which showed near 100 % conversion for CO_2 and ~96% syngas selectivity at 950^oC.

The above-mentioned studies required high temperatures to achieve reasonable CO_2 conversions and syngas yields ($\geqslant$ 800 ^oC). However, high temperatures would increase the overall cost of operation and can lead to side reactions such as coke formation.[34] To improve the redox performance at low temperatures, the use of platinum group metals (PGMs) to enhance the catalytic activity of perovskite-based redox catalysts was proposed.[22,26] The primary role of PGMs is to activate CH_4. Haribal et al[26] demonstrated that Rh promoted, lanthanum doped cerium oxide can achieve near-complete CO_2 conversion with 83% syngas yield at 650^oC. However, PGMs would add significant cost to the catalyst. To address this, we reported a PGM free $LaNi_{0.35}Fe_{0.65}O_3$ (LNF)/$Ce_{0.85}Gd_{0.1}Cu_{0.05}O_{2-\delta}$ (CGCO) composite, which achieved >90% conversion for both the CO_2 splitting and methane partial oxidation (POx) steps at 750^oC, along

with >90% syngas selectivity in the methane POx step.[27] Although the synergy and compatibility between LNF and CGCO are highly beneficial for the activity of the redox catalyst, preparation of the composite oxides involves complex procedures. It is therefore desirable to further simplify the PGM-free redox catalyst to lower the cost while maintaining its activity at intermediate temperatures. Another common limitation in the previous studies is that the stability of redox catalysts was demonstrated for a maximum of 100 cycles, and more typically 10 – 20 cycles. Verification of oxide stability over a larger number of cycles is important for potential industrial applications.

In this study, perovskite structured $LaNi_xFe_{1-x}O_3$, with nine different compositions (x = 0.05 – 0.5), were synthesized with an aim to simplify the redox catalyst formulation while maintaining its low temperature performance. In addition, rock salt structured $Ce_{0.85}Gd_{0.1}Cu_{0.05}O_{2-\delta}$ (CGCO) was also composited with the optimal LNF compositions to compare their performance. We also investigated the long-term stability of a $LaNi_{0.5}Fe_{0.5}O_3$ redox catalyst and unveiled the underlying reason for its gradual loss of activity. Based on the reactivation mechanism, air reoxidation was proposed and validated as an effective strategy to reverse such deactivation. With periodic reactivation, the LNF redox catalyst exhibited stable performance over 900 cycles, highlighting its potential as a cost-effective redox catalyst for the hybrid redox process.

2. Experimental

2.1. Redox catalyst synthesis

$LaNi_xFe_{1-x}O_{3-\delta}$ perovskites were prepared via a modified Pechini method. The detailed synthesis procedure was described elsewhere[27]. The main synthesis steps include mixing nitrate precursors of La, Ni and Fe with citric acid at molar ratio of 1: 2.5 (sum of metal cations: acetic acid). This is followed by mixing the dissolved cations with ethylene glycol at a 1.5:1 molar ratio (ethylene glycol: citric acid). The resulting mixture is then heated at 80 ^{o}C to form a gel. The gel was first dried at 120 ^{o}C overnight then calcined at 750 ^{o}C for 6 h under an oxidative environment. Mixed composites were prepared by first synthesizing CGCO separately, using the modified Pechini method, and mixing it with LNF at a 60/40 ratio by weight using a high-energy ball mill. This is

following by pelletization. Finally, all the prepared sample were fragmented and sieved to a size range of 250-450 µm for redox experiments in a fixed bed (U-shaped quartz tube; 4mm ID). Standalone LNF and composite CGCO/LNF were also synthesized for redox experiments in a 0.75" I.D. packed bed with a larger particle size range (850 µm-1,000 µm).

2.2. Characterization

Crystalline phases in various samples, including as-prepared, deactivated, reactivated, and O_2/CO_2 treated samples, were characterized via X-ray diffraction (XRD). Rigaku SmartLab X-ray diffractometer with Cu-Kα radiation at 40 kV and 44 mA was used to record the diffraction spectra. A step-size method with a step size of 0.05° and a residence time of 2 s at each step was used by varying the 2θ angle from 20° to 80°. Temperature-programmed reduction/Oxidation (TPR/TPO) experiments were performed to investigate the reducibility and deactivation/re-activation mechanisms. In TGA based TPR/TPO experiments, ~10 mg of sample was placed inside a thermogravimetric analyser (TGA) apparatus. For TPR, the samples were exposed to 200 ml/min of CH_4/Ar mixture (5 vol%) with a temperature ramping rate of 20 ^oC/min. TPO experiments were performed in both a fixed bed (U-shaped quartz tube; 4mm ID) and a TGA by exposing the deactivated sample to O_2/Ar or CO_2/Ar mixture (5 vol%) at 200 ml/min and 25 ml/min respectively with a temperature ramping rate of 20 ^oC/min. Scanning electron microscopy (SEM) and energy dispersive X-ray spectroscopy (EDS) analyses were performed using a Hitachi S3200 VPSEM with an acceleration voltage of 20kVa.

2.3. Redox tests

The redox performance of all the samples prepared was evaluated by exposing them to CH_4/CO_2 redox cycles. In a typical experiment, the sample was packed in a in a fixed bed (U-shaped quartz tube; 4mm ID) which was placed inside an electric furnace. The product gas compositions were quantified with a quadrupole mass spectrometer (Cirrus 2, MKS). 0.5g of the as prepared redox catalyst sizing between 250-450um was loaded into the U-shaped quartz tube. To keep the particles in place, U-tube was loaded with quartz wool on both ends. The furnace was heated up to reaction temperature in Ar (25 ml/min) followed by the introduction of reducing gas CH_4 at 2.8 ml/min for 2 mins. After the reduction step, the U-tube was purged with 25 ml/min Ar to

remove the leftover CH_4 followed by the introduction of CO_2 at 1.4 ml/min along with 25 ml/min Ar for 4 mins. This is followed with Ar purge prior to the next redox cycle.

A 0.75" I.D. packed bed was used for long-term stability studies with 5g of redox catalysts (both standalone LNF and composite CGCO/LNF). A schematic of the reactor is provided in Figure S1 (in the Supplementary Information). Before the long-term experiments, the effect of gas hourly space velocities (GHSV) was determined with 80% CH_4 and CO_2 as the reducing and oxidizing gases respectively. A schematic of the packed bed is shown in the Figure S1. The total volumes of reducing (112.5cm^3) and oxidizing (112.5cm^3) gases injected were kept constant by adjusting the contact time at various GHSVs (1673, 835 and 420h^{-1}). Long term testing was performed with 10g LNF for 900 cumulative cycles. For the first 500 cycles, CH_4 and CO_2 concentrations were 30% and 50% respectively. Cycles 501-700 were conducted with 15% CH_4 and CO_2 concentrations. Cycles 701 to 900 were performed with 15% CH_4 and CO_2 with 20 ml total injection for both CH_4 and CO_2. To re-activate the redox catalyst, air treatment of the redox catalyst was implemented periodically at an overall air flow rate of 45 ml/min for 25 minutes at 930 ^oC.

3. Results and Discussion

3.1. Phase Characterization and redox performance of the redox catalysts

XRD patterns of the as synthesised $LaNi_xFe_{1-x}O_{3-\delta}$ samples are shown in Figure 2. For all the $LaNi_xFe_{1-x}O_{3-\delta}$ samples, an orthorhombic perovskite phase was detected with negligible impurities. This confirms the compatibility of Ni as a B-site dopant in $LaFeO_3$. Redox performance of the as prepared samples was evaluated in the lab scale U-tube reactor by exposing them to CH_4/CO_2 redox cycles, as shown in Figure 3. As can be seen, partial substitution of Ni into $LaFeO_3$ substantially improved the redox performance in both methane and CO_2 conversion steps: CH_4 conversion was merely 15% for $LaFe_{0.05}Ni_{0.95}O_3$. Increase in the Ni content improved the redox performance by up to 6 folds. The best performance was observed for $LaNi_{0.4}Fe_{0.6}O_3$ and $LaNi_{0.5}Fe_{0.5}O_3$, with near 90% CH_4 and CO_2 conversions. CO selectivities for these samples were also near 90%. $LaNi_{0.5}Fe_{0.5}O_3$ exhibited slightly higher activity than $LaNi_{0.4}Fe_{0.6}O_3$. We note that small amounts of coke were also formed during the methane POx step on all the samples. Figure 3(b) summarizes the H_2/CO ratios and the amounts of coke formation in the methane POx step.

As can be seen, H_2/CO for $LaNi_{0.4}Fe_{0.6}O_3$ and $LaNi_{0.5}Fe_{0.5}O_3$ was near 2.4. Mass balances indicate 0.07 and 0.08 wt.% coke formation, respectively. We note that the coke formed in the methane POx step was near completely gasified in the CO_2-splitting step, leading to increased CO yield when compared to the redox based CO_2-splitting alone. Generally speaking, the amount of carbon deposition is affected by the amount of CH_4 injected and hence it varies with the reaction time of the POx step. Figure S2 in the supplemental file illustrates the accumulation of coke over time on $LaNi_{0.5}Fe_{0.5}O_3$. The redox catalysts tested in the current study resulted in relatively small amounts of carbon (0.45 to 0.8mg/g. catalyst/cycle) for the given reaction conditions, as shown in Figure 3b. A majority of this carbon, ~81% in the case of $LaNi_{0.5}Fe_{0.5}O_3$, was gasified in the subsequent CO_2-splitting step. Further discussions on coke formation, removal, and long-term accumulation are provided in Section 3.3. It should also be noted that the coke formation for $LaNi_{0.35}Fe_{0.65}O_3$ was lower than $LaNi_{0.4}Fe_{0.6}O_3$ and $LaNi_{0.5}Fe_{0.5}O_3$, but the corresponding CH_4/CO_2 conversions were significantly lower as well. The general trends from Figure 3 indicate that an increase in nickel content leads to improved redox performance. On the other hand, it also leads to moderate increase in coke formation. This is understandable given that Ni is more reducible than Fe and metallic Ni (and Ni-Fe bimetallic alloys) are highly active for methane activation and coke formation. In addition, there appeared to be a few "outliers", e.g. $LaNi_{0.35}Fe_{0.65}O_3$ and $LaNi_{0.15}Fe_{0.85}O_3$, especially in terms of the trend for coke formation amount. This is likely to have resulted from the slight differences in the average oxidation states of the redox catalysts when operated under steady state redox cycles. Redox catalysts stabilized at higher average oxidation states tend to exhibit lower activity for methane activation and hence lower coke formation.

In our previous study, we showed that $LaNi_{0.35}Fe_{0.65}O_3$ (LNF)/$Ce_{0.85}Gd_{0.1}Cu_{0.05}O_{2-\delta}$ (CGCO) composite exhibited satisfactory performance with >90% conversions in both methane partial oxidation (POx) and CO_2 splitting steps and with >95% CO selectivity at 750°C.[27] In comparison, $LaNi_{0.4}Fe_{0.6}O_3$ and $LaNi_{0.5}Fe_{0.5}O_3$ exhibited similar performance at a lower temperature (700°C). Given the simplicity of $LaNi_{0.4}Fe_{0.6}O_3$ and $LaNi_{0.5}Fe_{0.5}O_3$ compared to LNF/CGCO composites, they can be more cost-effective for HRP. The next section investigates the effect of CGCO addition to $LaNi_{0.4}Fe_{0.6}O_3$ and $LaNi_{0.5}Fe_{0.5}O_3$ towards the redox performance.

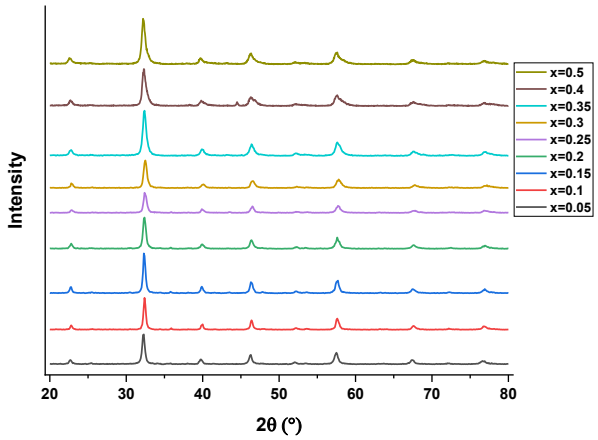

Figure 2. *XRD Patterns of as-synthesized $LaNi_xFe_{1-x}O_{3-\delta}$ (x = 0.05 to 0.5).*

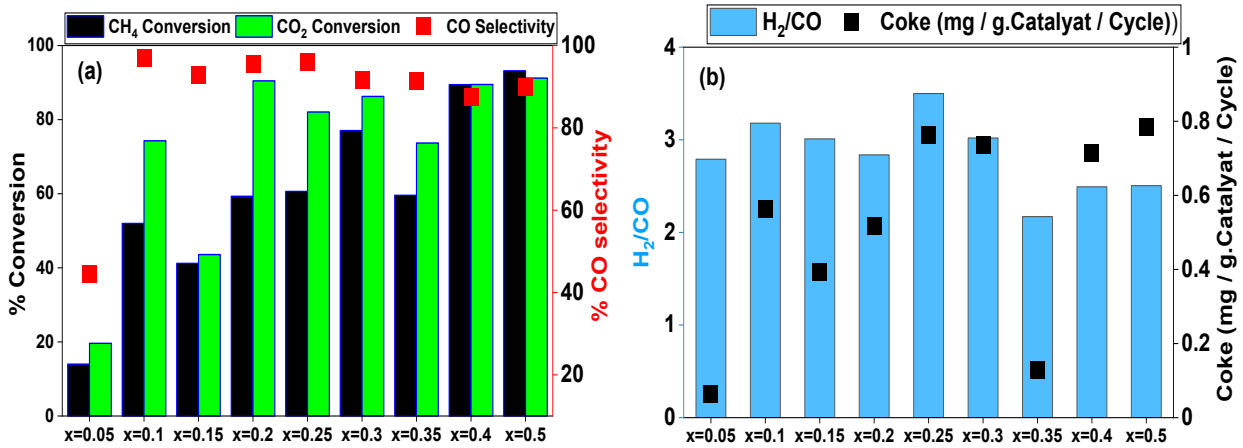

Figure 3. *Redox Performance of standalone $LaNi_xFe_{1-x}O_3$ (x = 0.05 to 0.5) at 700°C (a) CH_4 and CO_2 conversions and CO selectivity; (b) H_2/CO ratios and amount of coke formation.*

3.2. Redox performance comparisons between standalone LNF and LNF/CGCO composites

Our previous study indicated that CGCO effectively enhances the redox performance of $LaNi_{0.35}Fe_{0.65}O_3$. To analyze and compare the redox performance of standalone $LaNi_{0.4}Fe_{0.6}O_3$ and $LaNi_{0.5}Fe_{0.5}O_3$ with LNF/CGCO mixed composites, CGCO was mixed with $LaNi_{0.4}Fe_{0.6}O_3$ and $LaNi_{0.5}Fe_{0.5}O_3$, to prepare two CGCO/LNF redox catalysts. Before running the redox tests, the mixed composites were reduced in CH_4 to evaluate the reducibility. The results are shown in Figure 4. Three peaks were observed. The first peak is very prominent for all the samples whereas the second peak exhibits as a shoulder. These two peaks correspond to the reduction of metal

cations. The first peak is likely to be the reduction of Fe^{3+} to Fe^{2+} and Ni^{3+} to Ni^{2+} whereas the second peak can be assigned to the further reduction to metallic phases.[41] CGCO, on the other hand, is hardly reducible at temperatures less than 800 °C. However, the synergistic effect of the LNF/CGCO composite would facilitate its reduction.[27] The addition of CGCO clearly shifted the reduction peaks of $LaNi_{0.4}Fe_{0.6}O_3$/CGCO and $LaNi_{0.5}Fe_{0.5}O_3$/CGCO to lower temperatures, by 14 and 54 °C, respectively. In addition, the total weight loss for $LaNi_{0.4}Fe_{0.6}O_3$, $LaNi_{0.5}Fe_{0.5}O_3$, $LaNi_{0.4}Fe_{0.6}O_3$/CGCO and $LaNi_{0.5}Fe_{0.5}O_3$/CGCO were 8.5, 5, 5.7 and 2.3wt%. The total weight loss numbers indicate that although the addition of CGCO shifted the reduction peaks to lower temperatures, the oxygen capacities of standalone LNFs are higher. This is understandable since CGCO is less reducible. The total weight loss during the reduction was above 5 wt% for all the samples except for $LaNi_{0.5}Fe_{0.5}O_3$ /CGCO. The third peak, which corresponds to weight gain, was observed due to the coke deposition via CH_4 cracking. It is evident that addition of CGCO was effective to inhibit coke formation.

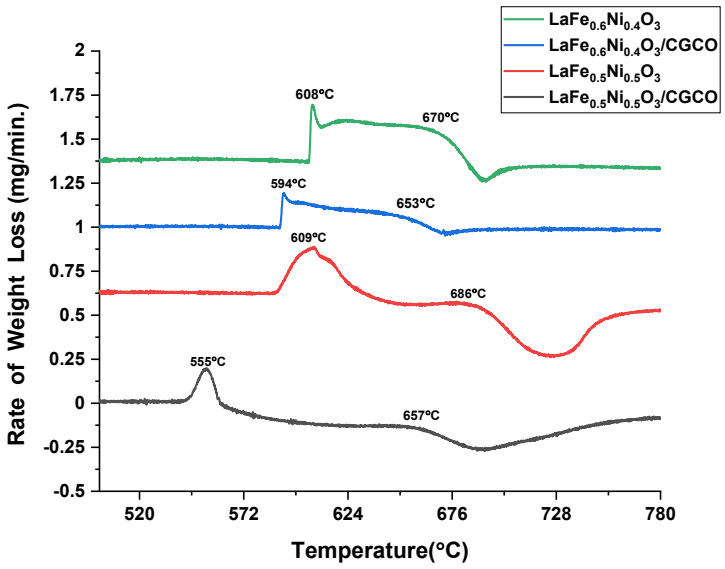

Figure 4. *CH_4 TPR of standalone LNF and Composite LNF/CGCO (40/60)*

The TPR peaks also confirm that all the materials are reducible at temperatures less than 700 °C. Meanwhile, equilibrium limitations for methane conversion would likely to require an operating temperature higher than 650 °C. As such, standalone LNFs, which were substantially reduced by 680°C based on TPR, are likely to exhibit satisfactory performance despite being less reducible

than CGCO/LNF composites. In addition, coke formation should be relatively low at operating temperatures below 700 ^{o}C. To compare the redox performance under isothermal conditions, both composite materials (CGCO/LNF) and standalone LNFs ($LaNi_{0.4}Fe_{0.6}O_3$ and $LaNi_{0.5}Fe_{0.5}O_3$,) were evaluated in the lab scale U-tube reactor under identical conditions. The redox performance of mixed composites is shown in Figure 5a. It can be observed that, in the case of $LaNi_{0.4}Fe_{0.6}O_3$ and $LaNi_{0.5}Fe_{0.5}O_3$, the addition of CGCO improved the redox performance with approximately 4% increase in the CH_4 conversion and 3% increase in the CO_2 conversion. Coke formation was also higher (~30%) for standalone LNF compared to the composite CGCO/LNF (Figure 5b). The higher coke resistance of CGCO/LNF samples is consistent with the TPR results. We note that the redox performances of standalone LNFs are only slightly inferior to those of the composite CGCO/LNFs. Considering the simplicity and potential cost savings, standalone $LaNi_{0.5}Fe_{0.5}O_3$ can be a very promising candidate. It is also noted that the redox kinetics can affect the redox catalyst performance at high gas hourly space velocities (GHSVs). It is therefore informative to investigate the effect of CGCO addition at a larger scale. With this in mind, we tested both standalone $LaNi_{0.5}Fe_{0.5}O_3$(LNF) and composite CGCO/LNF in a .75" I.D. packed bed at 700 °C with 80% CH_4/CO_2 concentrations (balance Argon). The results are shown in the Figure 6. It was found that GHSV has a significant influence on the syngas yield. For example, at GHSV=1670 h^{-1} and 15s injection time, 63.65% CH_4 conversion, 58.85% CO_2 conversion and 95.25% CO selectivity was observed, respectively. By decreasing the GHSV to 835 h^{-1}, syngas yield was improved, with 71.30% CH_4 conversion, 72.23% CO_2 conversion, and 93.84% CO selectivity. Upon further decrease of GHSV, redox performance was further improved to 76.51% CH_4 conversion, 82.14% CO_2 conversion and 91.40% CO selectivity. Improved performance at lower GHSVs is due to the longer residence time for the reactant gases. We also note that the redox performance of composite CGCO/LNF is comparable to that of standalone LNF. This further confirms the potential of standalone LNF as a simple yet effective redox catalyst.

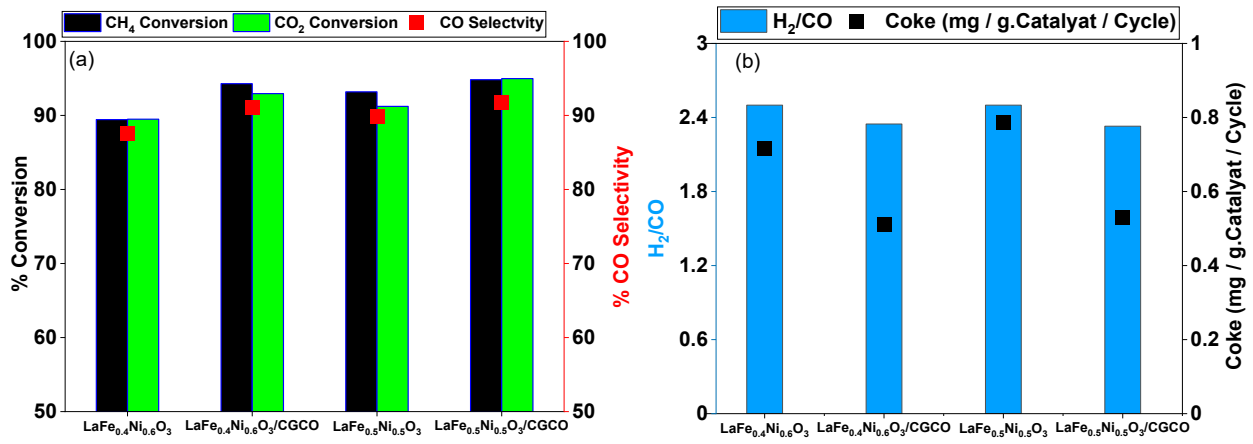

Figure 5. *Redox Performance of standalone $LaNi_xFe_{1-x}O_{3-\delta}$ (x = 0.4 and 0.5) and composite LNF/CGCO (40/60) at 700^{0}C (a) CH_4 and CO_2 conversions and CO selectivity in the methane POx step; (b) H_2/CO ratio and coke formation.*

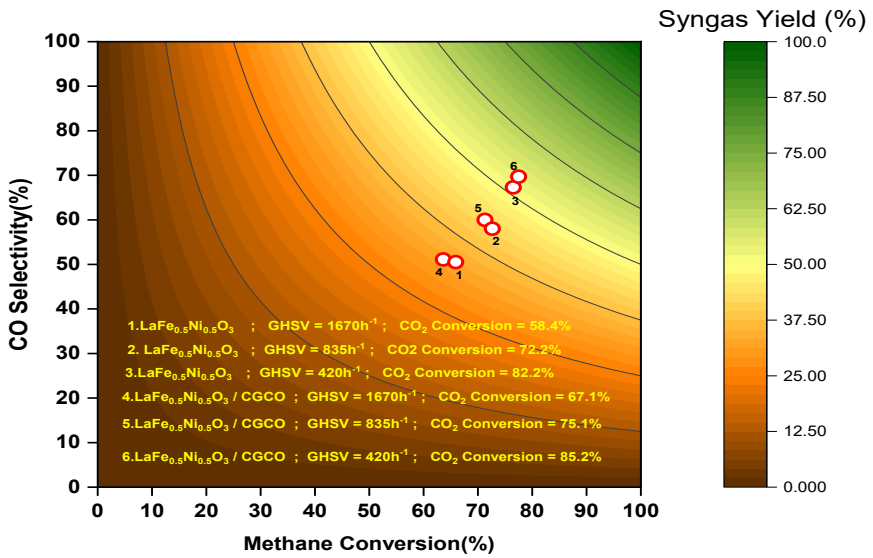

Figure 6. *Effect of GHSV on the redox performance of standalone LNF and Composite LNF/CGCO (40/60) in a 0.75" I.D. packed bed at 700 °C with 80% CH_4 and CO_2 concentrations in the feed.*

3.3. Redox catalyst deactivation and reactivation mechanisms and long-term stability

To evaluate the long-term stability of the redox catalyst, a 0.75" I.D. packed bed reactor was used. A 700-cycle experiment was first performed. Results are shown in the Figure 7 (cycle to cycle data is provided in the Figure S3). As can be seen, both CH_4 and CO_2 conversions started at ~86 and 92% respectively. At the 500th cycle, conversions dropped to ~80%, indicating a slight deactivation of the redox catalyst. It was determined that deep oxidation of the redox catalyst

with air was effective in reactivating the redox catalyst. As can be seen, reactivation of the redox catalyst with air prior to cycle 501 resulted in a 5% increase in methane conversion and 6% increase in CO_2 conversion. To investigate the effect of inlet gas concentrations, both CH_4 and CO_2 concentrations were decreased to 15% starting from cycle 501 without changing the total amount of CH_4 and CO_2 being injected. As can be seen, both CH_4 and CO_2 conversions started at above 85% after reactivation and then gradually dropped to ~80% at the 700th cycle. This indicates that gradual deactivation may be unavoidable without periodic reactivation of the LNF redox catalyst. Before further exposing the sample for additional redox cycles, deactivation/re-activation mechanisms were investigated.

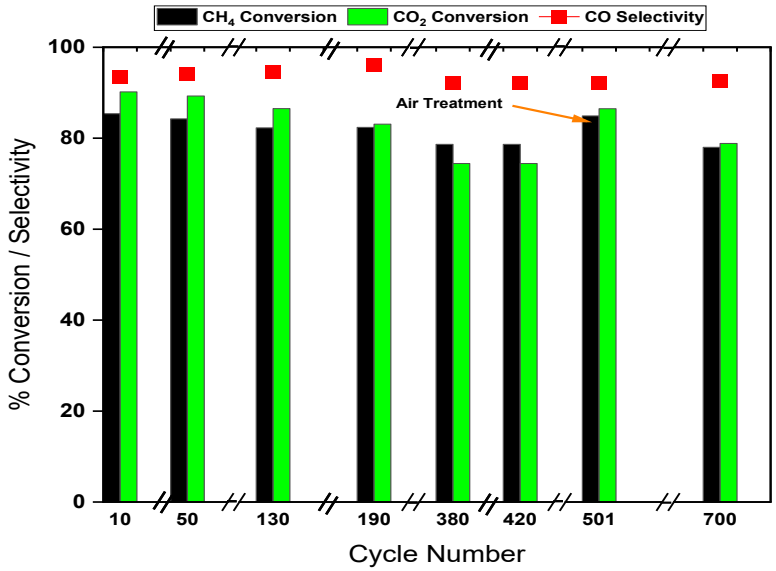

Figure 7. *CH_4/CO_2 conversions and CO selectivity for long term tests with a standalone $LaNi_{0.5}Fe_{0.5}O_3$.*

To determine the re-activation and deactivation mechanisms, XRD and temperature programmed oxidation with O_2 and CO_2 were performed. Figure 8a and 8b show the gas evolutions during O_2-TPO and the CO_2-TPO of the deactivated redox catalyst, respectively. It can be observed that for the case of O_2-TPO, the product CO_2 appears at around 665°C, whereas for CO_2-TPO, this peak was shifted to 710°C. This is due to the lower activity of CO_2 for carbon gasification. More importantly, the carbon removed from CO_2-TPO (40 mg/g of redox catalyst)

was roughly 1/3 of the carbon removable by O_2-TPO (130 mg/g). This is also consistent with the TGA based TPO results (Figure S4) and SEM/EDX analysis (Figure S5). From a thermodynamic standpoint, both graphitic and amorphous carbon should be removed by CO_2 at temperatures below 900 ^oC.[42,43] This indicates the formation of carbon species that are largely inert to CO_2 and hence cannot be effectively removed by CO_2 regeneration in typical redox steps. XRD characterization of the samples, as will be discussed in the next paragraph, indicates that these CO_2 stable species should be iron carbides. It is also worth noting that the net carbon accumulation is 0.325 mg/gram of redox catalyst each cycle. This indicates that the net carbon build-up in each cycle is small and most of the amorphous and graphic carbon species are gasified during the CO_2 regeneration step. amount

Figure 8c shows the XRD Patterns of the samples at various stages of the reactions. As can be seen, the deactivated samples, both after methane reduction and CO_2 regeneration, contain significant amount of iron carbides (Fe_3C and/or Fe_5C_2). Exposure to CO_2 appears to have promoted the formation of Fe_5C_2 but was unable to remove the iron bond carbon within the sample. In contrast, iron carbide species are completely absent from the reactivated (air treated sample). Moreover, the monoclinic Fe_5C_2 phase, although insignificant, start to form within 5 redox cycles after reactivation with air. These findings indicate that accumulation of iron carbide phases is likely to be the primary cause for deactivation. It is also noted that the deactivated redox catalyst exhibits larger crystallite sizes for the La_2O_3 phase (44.7 nm) whereas the reactivated sample after 5 redox cycles showed considerably smaller La_2O_3 crystallite size (37 nm). Meanwhile, the LNF phase crystallite size remained nearly identical at 56.8 nm. This sintering of the La_2O_3 phase is likely to have resulted from the continuous depletion of Fe due to the formation of the “inert” carbide phase. We note that the reversible solid-state reaction between Fe and La_2O_3 represents a key pathway for lattice oxygen release and uptake during cyclic methane conversion and CO_2-splitting. The continuous depletion of Fe to the carbide phases would hence lead to (i) sintering of the unreacted La_2O_3 phase; (ii) loss of redox activity. XRD spectra also indicates the formation of $FeNi_3$ phase, which is effective for methane activation, in the redox catalysts under working conditions.

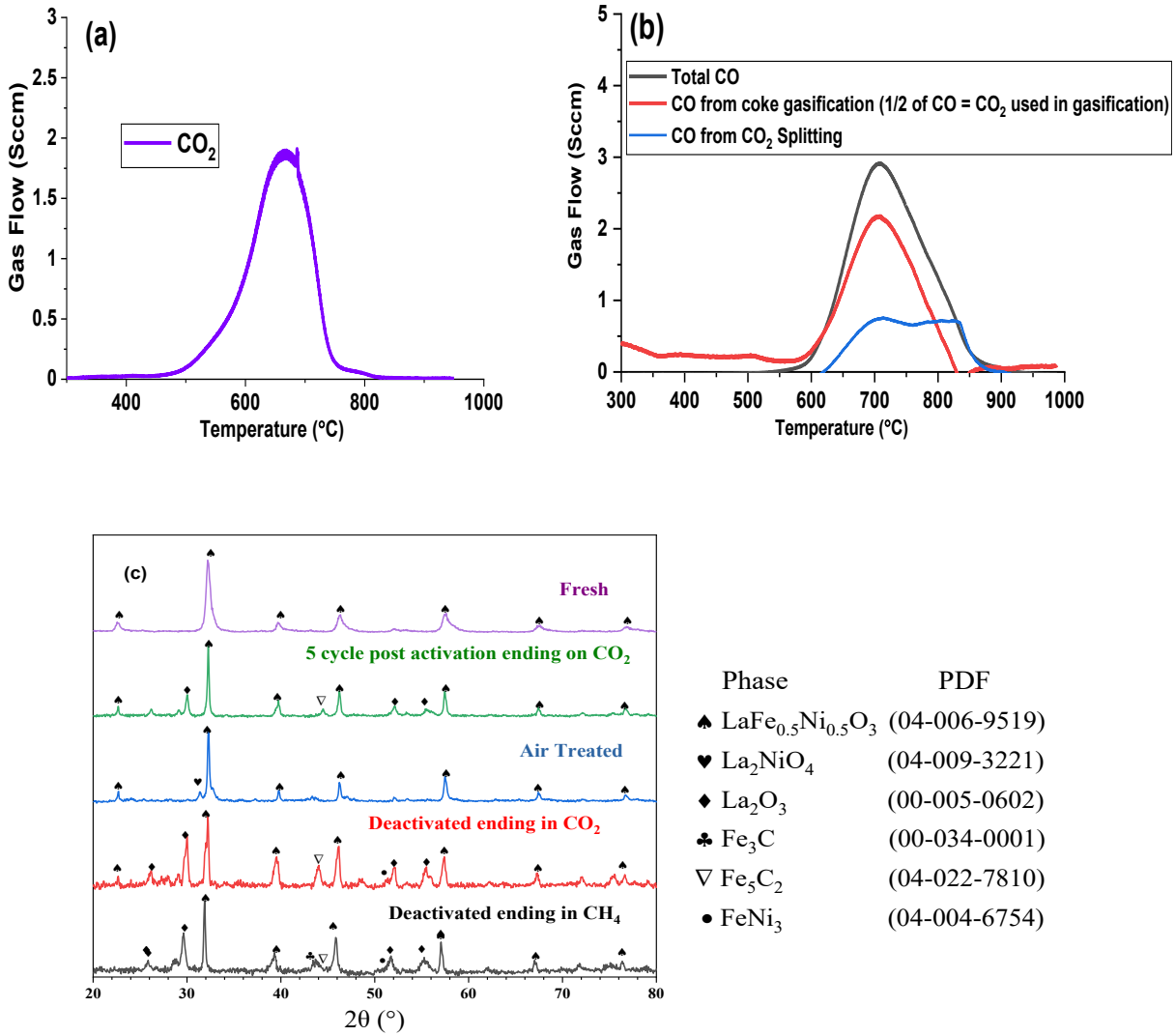

***Figure 8**. Redox catalyst characterizations. (a) Product gas evolution during O_2-TPO of the deactivated redox catalyst; (b) Product gas evolution during CO_2-TPO of the deactivated redox catalyst; (c) XRD of deactivated and reactivated LNF redox catalyst at various stages.*

From the above experimental results and characterizations, it can be concluded that gradual deactivation of the LNF redox catalyst, albeit very slow, is unavoidable due to the formation of the carbide phase. In addition, reactivation with air is highly effective to restore its redox activity. To validate the effectiveness of this reactivation strategy, we operated the redox catalyst for an additional 200 cycles. During this experiment, the redox catalyst was re-oxidized with air every 40 cycles. As shown in Figure 9, >85% methane conversion, 95% CO selectivity, and ~90% CO_2

conversion were achieved throughout the last 200 cycles with periodic reactivation. Considering that the LNF redox catalyst has experienced over 900 cumulative redox cycles, the results demonstrates the long-term stability of the redox catalyst when periodic reactivation with air is implemented. We also note that infrequent air reactivation, i.e. once every 40 - 50 cycles, will have a minimal negative impact on the overall syngas and CO yields.

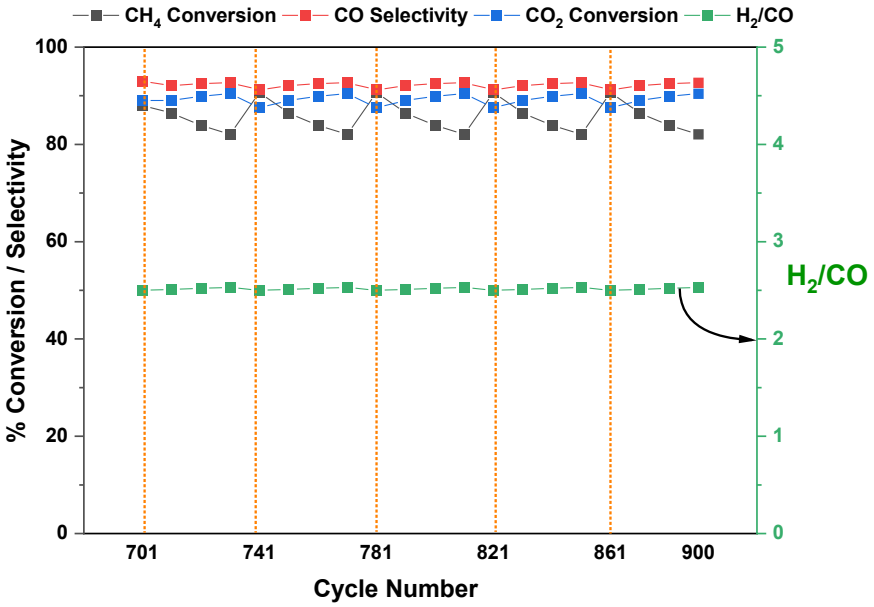

Figure 9. *Long-term redox performance of the LNF redox catalyst with air reactivation every 40 cycles (orange dashed line indicates air treatment prior to the specified cycle number).*

4. Conclusion

The present study investigates perovskite structured $LaNi_xFe_{1-x}O_{3-\delta}$ (LNF) as redox catalysts for redox based CO_2-splitting and methane partial oxidation at relatively low temperatures (~700 °C). Specifically, nine $LaNi_xFe_{1-x}O_{3-\delta}$ samples with x ranging from 0.05 to 0.5 were prepared and evaluated. Among them, $LaNi_{0.4}Fe_{0.6}O_3$ and $LaNi_{0.5}Fe_{0.5}O_3$ were determined to be the most active for the redox reactions, showing >90% CH_4 conversion and CO selectivity in the methane POx step and >90% CO yield in the CO_2-splitting step at 700 °C. The redox performance of the standalone $LaNi_{0.4}Fe_{0.6}O_3$ and $LaNi_{0.5}Fe_{0.5}O_3$ redox catalysts compared favorably with that of $Ce_{0.85}Gd_{0.1}Cu_{0.05}O_{2-\delta}$ (CGCO) promoted LNF redox catalysts. A long-term redox test of $LaNi_{0.5}Fe_{0.5}O_3$ indicates that the redox catalyst gradually loses its activity over repeated redox cycles, resulting in a 6% drop in methane conversion (from 86%) over 500 cycles. Reoxidation of the partially deactivated redox catalyst with air was found to be effective to restore its activity. The deactivation mechanism was determined to be the formation and slow accumulation of iron carbide (Fe_3C and Fe_5C_2) phases, which cannot be effectively removed by the CO_2 splitting step. As such, periodic reactivation with air, e.g. every 40 – 50 redox cycles, was proposed as a strategy to maintain the long-term stability of the redox catalyst. Such a strategy was verified to be effective, as confirmed by operating the redox catalyst over 900 cumulative cycles while maintaining satisfactory redox performance.

Supporting Information

Supporting Information is available free of charge on the ACS Publications website. The supporting information includes the packed bed reactor set up, coke accumulation profile during the methane POx step, cycle to cycle data for the packed bed experiment, O_2/CO_2-TPO of the deactivated redox catalyst, and SEM/EDX images.

Acknowledgment

This work was supported by the U.S. Department of Energy (Award No. DE-FE0031703), National Science Foundation (CBET- 1923468), and the North Carolina State University Kenan Institute for

Engineering, Technology and Science. We acknowledge the use of the Analytical Instrumentation Facility (AIF) at North Carolina State University, which is supported by the State of North Carolina and the National Science Foundation.

References

(1) Bert Metz, Ogunlade Davidson, Heleen de Coninck, Manuela Loos and Leo Meyer (Eds.) ; Carbon Dioxide Capture and Storage. Cambridge University Press. IPCC. 2005 IP, UK. pp 431.

(2) Newell, R. G.; Raimi, D.; Aldana, G. Global Energy Outlook 2019: The Next Generation of Energy. 46. https://media.rff.org/documents/GEO_Report_8-22-19.pdf. Accessed on 06/04/2021.

(3) Inventory of U.S. Greenhouse Gas Emissions and Sinks. 2021. https://www.epa.gov/ghgemissions/inventory-us-greenhouse-gas-emissions-and-sinks. Accessed on 06/04/2021.

(4) Fatih Birol, *World Energy Outlook 2012*; International Energy Agency, Ed.; World Energy Outlook; Paris, https://www.iea.org/reports/world-energy-outlook-2012. Accessed on 06/04/2021.

(5) Ho, H.-J.; Iizuka, A.; Shibata, E. Carbon Capture and Utilization Technology without Carbon Dioxide Purification and Pressurization: A Review on Its Necessity and Available Technologies. *Ind. Eng. Chem. Res.* **2019**, *58* (21), 8941–8954. https://doi.org/10.1021/acs.iecr.9b01213.

(6) Review of Post-Combustion Carbon Dioxide Capture Technologies Using Activated Carbon. https://www.sciencedirect.com/science/article/abs/pii/S1001074218325622 Accessed on 06/04/2021.

(7) Daza, Y. A.; Kuhn, J. N. CO_2 Conversion by Reverse Water Gas Shift Catalysis: Comparison of Catalysts, Mechanisms and Their Consequences for CO_2 Conversion to Liquid Fuels. *RSC Adv.* **2016**, *6* (55), 49675–49691. https://doi.org/10.1039/C6RA05414E.

(8) Rajabi, M.; Mehrpooya, M.; Haibo, Z.; Huang, Z. Chemical Looping Technology in CHP (Combined Heat and Power) and CCHP (Combined Cooling Heating and Power) Systems: A Critical Review. *Applied Energy* **2019**, *253*, 113544. https://doi.org/10.1016/j.apenergy.2019.113544.

(9) Du, C.; Lu, P.; Tsubaki, N. Efficient and New Production Methods of Chemicals and Liquid Fuels by Carbon Monoxide Hydrogenation. *ACS Omega* **2020**, *5* (1), 49–56. https://doi.org/10.1021/acsomega.9b03577.

(10) Mesters, C. A Selection of Recent Advances in C1 Chemistry. *Annu. Rev. Chem. Biomol. Eng.* **2016**, *7* (1), 223–238. https://doi.org/10.1146/annurev-chembioeng-080615-034616.

(11) Peter, S. C. Reduction of CO_2 to Chemicals and Fuels: A Solution to Global Warming and Energy Crisis. *ACS Energy Lett.* **2018**, *3* (7), 1557–1561. https://doi.org/10.1021/acsenergylett.8b00878.
(12) Muhich, C.; Steinfeld, A. Principles of Doping Ceria for the Solar Thermochemical Redox Splitting of H_2O and CO_2. *J. Mater. Chem. A* **2017**, *5* (30), 15578–15590. https://doi.org/10.1039/C7TA04000H.
(13) Carrillo, A. J.; Bork, A. H.; Moser, T.; Sediva, E.; Hood, Z. D.; Rupp, J. L. M. Modifying $La_{0.6}Sr_{0.4}MnO_3$ Perovskites with Cr Incorporation for Fast Isothermal CO_2-Splitting Kinetics in Solar-Driven Thermochemical Cycles. *Adv. Energy Mater.* **2019**, *9* (28), 1803886. https://doi.org/10.1002/aenm.201803886.
(14) Furler, P.; Scheffe, J.; Marxer, D.; Gorbar, M.; Bonk, A.; Vogt, U.; Steinfeld, A. Thermochemical CO_2 Splitting *via* Redox Cycling of Ceria Reticulated Foam Structures with Dual-Scale Porosities. *Phys. Chem. Chem. Phys.* **2014**, *16* (22), 10503–10511. https://doi.org/10.1039/C4CP01172D.
(15) Arifin, D.; Aston, V. J.; Liang, X.; McDaniel, A. H.; Weimer, A. W. CoFe2O4 on a Porous Al2O3 Nanostructure for Solar Thermochemical CO2 Splitting. *Energy Environ. Sci.* **2012**, *5* (11), 9438. https://doi.org/10.1039/c2ee22090c.
(16) Chueh, W. C.; Falter, C.; Abbott, M.; Scipio, D.; Furler, P.; Haile, S. M.; Steinfeld, A. High-Flux Solar-Driven Thermochemical Dissociation of CO2 and H2O Using Nonstoichiometric Ceria. *Science* **2010**, *330* (6012), 1797–1801. https://doi.org/10.1126/science.1197834.
(17) Al-Shankiti, I.; Ehrhart, B. D.; Weimer, A. W. Isothermal Redox for H_2O and CO_2 Splitting – A Review and Perspective. *Solar Energy* **2017**, *156*, 21–29. https://doi.org/10.1016/j.solener.2017.05.028.
(18) Tong, A.; Zeng, L.; Kathe, M. V.; Sridhar, D.; Fan, L.-S. Application of the Moving-Bed Chemical Looping Process for High Methane Conversion. *Energy Fuels* **2013**, *27* (8), 4119–4128. https://doi.org/10.1021/ef3020475.
(19) Mattisson, T.; Lyngfelt, A. Applications of Chemical-Looping Combustion with Capture of CO2. Second Nordic Minisymposium on Carbon Dioxide Capture and Storage, Göteborg, Sweden, October 26, 2001, 6.
URL: http://www.entek.chalmers.se/anly/symp/symp2001.html
(20) Li, D.; Xu, R.; Gu, Z.; Zhu, X.; Qing, S.; Li, K. Chemical-Looping Conversion of Methane: A Review. *Energy Technol.* **2020**, *8* (8), 1900925. https://doi.org/10.1002/ente.201900925.
(21) Bhavsar, S.; Najera, M.; Veser, G. Chemical Looping Dry Reforming as Novel, Intensified Process for CO2 Activation. *Chem. Eng. Technol.* **2012**, *35* (7), 1281–1290. https://doi.org/10.1002/ceat.201100649.
(22) Araiza, D. G.; Arcos, D. G.; Gómez-Cortés, A.; Díaz, G. Dry Reforming of Methane over Pt-Ni/CeO2 Catalysts: Effect of the Metal Composition on the Stability. *Catalysis Today* **2021**, *360*, 46–54. https://doi.org/10.1016/j.cattod.2019.06.018.
(23) Adanez, J.; Abad, A.; Garcia-Labiano, F.; Gayan, P.; de Diego, L. F. Progress in Chemical-Looping Combustion and Reforming Technologies. *Progress in Energy and Combustion Science* **2012**, *38* (2), 215–282. https://doi.org/10.1016/j.pecs.2011.09.001.
(24) Kang, D.; Lim, H. S.; Lee, J. W. Mesoporous Fe_2O_3–CeO_2–Al_2O_3 Redox catalyst for Chemical Looping Dry Reforming with Subsequent Water Splitting. *Ind. Eng. Chem. Res.* **2020**, *59* (36), 15912–15920. https://doi.org/10.1021/acs.iecr.0c03197.

(25) Hosseini, D.; Abdala, P. M.; Donat, F.; Kim, S. M.; Müller, C. R. Bifunctional Core-Shell Architecture Allows Stable H2 Production Utilizing CH4 and CO2 in a Catalytic Chemical Looping Process. *Applied Catalysis B: Environmental* **2019**, *258*, 117946. https://doi.org/10.1016/j.apcatb.2019.117946.
(26) Haribal, V. P.; Wang, X.; Dudek, R.; Paulus, C.; Turk, B.; Gupta, R.; Li, F. Modified Ceria for "Low-Temperature" CO_2 Utilization: A Chemical Looping Route to Exploit Industrial Waste Heat. *Adv. Energy Mater.* **2019**, *9* (41), 1901963. https://doi.org/10.1002/aenm.201901963.
(27) Jiang, Q.; Gao, Y.; Haribal, V. P.; Qi, H.; Liu, X.; Hong, H.; Jin, H.; Li, F. Mixed Conductive Composites for 'Low-Temperature' Thermo-Chemical CO2 Splitting and Syngas Generation. *J. Mater. Chem. A* **2020**, *8* (26), 13173–13182. https://doi.org/10.1039/D0TA03232H.
(28) Teimouri, Z.; Abatzoglou, N.; Dalai, A. K. Kinetics and Selectivity Study of Fischer–Tropsch Synthesis to C5+ Hydrocarbons: A Review. *Catalysts* **2021**, *11* (3), 330. https://doi.org/10.3390/catal11030330.
(29) Sunley, G. J.; Watson, D. J. High Productivity Methanol Carbonylation Catalysis Using Iridium The CativaTM Process for the Manufacture of Acetic Acid. *Catalysis Today* **2000**, 15.
(30) Lyngfelt, A. Chemical-Looping Combustion of Solid Fuels – Status of Development. *Applied Energy* **2014**, *113*, 1869–1873. https://doi.org/10.1016/j.apenergy.2013.05.043.
(31) Mishra, A.; Li, F. Chemical Looping at the Nanoscale — Challenges and Opportunities. *Current Opinion in Chemical Engineering* **2018**, *20*, 143–150. https://doi.org/10.1016/j.coche.2018.05.001.
(32) Zeng, L.; Cheng, Z.; Fan, J. A.; Fan, L.-S.; Gong, J. Metal Oxide Redox Chemistry for Chemical Looping Processes. *Nat Rev Chem* **2018**, *2* (11), 349–364. https://doi.org/10.1038/s41570-018-0046-2.
(33) More, A.; Bhavsar, S.; Veser, G. Iron–Nickel Alloys for Carbon Dioxide Activation by Chemical Looping Dry Reforming of Methane. *Energy Technol.* **2016**, *4* (10), 1147–1157. https://doi.org/10.1002/ente.201500539.
(34) Zhang, J.; Li, F. Coke-Resistant Ni@SiO2 Catalyst for Dry Reforming of Methane. *Applied Catalysis B: Environmental* **2015**, *176–177*, 513–521. https://doi.org/10.1016/j.apcatb.2015.04.039.
(35) Ratchahat, S.; Surathitimethakul, S.; Thamungkit, A.; Mala, P.; Sudoh, M.; Watanabe, R.; Fukuhara, C.; Chen, S. S.; Wu, K. C.-W.; Charinpanitkul, T. Catalytic Performance of Ni/CeO2 Catalysts Prepared from Different Routes for CO2 Methanation. *Journal of the Taiwan Institute of Chemical Engineers* **2021**, *121*, 184–196. https://doi.org/10.1016/j.jtice.2021.04.008.
(36) Deml, A. M.; Stevanović, V.; Holder, A. M.; Sanders, M.; O'Hayre, R.; Musgrave, C. B. Tunable Oxygen Vacancy Formation Energetics in the Complex Perovskite Oxide $Sr_x La_{1-x} Mn_y Al_{1-y} O_3$. *Chem. Mater.* **2014**, *26* (22), 6595–6602. https://doi.org/10.1021/cm5033755.
(37) Zhu, X.; Imtiaz, Q.; Donat, F.; Müller, C. R.; Li, F. Chemical Looping beyond Combustion – a Perspective. *Energy Environ. Sci.* **2020**, *13* (3), 772–804. https://doi.org/10.1039/C9EE03793D.

(38) Zhu, X.; Li, K.; Neal, L.; Li, F. Perovskites as Geo-Inspired Oxygen Storage Materials for Chemical Looping and Three-Way Catalysis: A Perspective. *ACS Catal.* **2018**, *8* (9), 8213–8236. https://doi.org/10.1021/acscatal.8b01973.
(39) Michalsky, R.; Neuhaus, D.; Steinfeld, A. Carbon Dioxide Reforming of Methane Using an Isothermal Redox Membrane Reactor. *Energy Technology* **2015**, *3* (7), 784–789. https://doi.org/10.1002/ente.201500065.
(40) Zhang, J.; Haribal, V.; Li, F. Perovskite Nanocomposites as Effective CO_2 -Splitting Agents in a Cyclic Redox Scheme. *Sci. Adv.* **2017**, *3* (8), e1701184. https://doi.org/10.1126/sciadv.1701184.
(41) Shah, S.; Sayono, S.; Ynzunza, J.; Pan, R.; Xu, M.; Pan, X.; Gilliard-AbdulAziz, K. L. The Effects of Stoichiometry on the Properties of Exsolved Ni-Fe Alloy Nanoparticles for Dry Methane Reforming. *AIChE J* **2020**, *66* (12). https://doi.org/10.1002/aic.17078.
(42) Xie, Y.; Yang, H.; Zeng, K.; Zhu, Y.; Hu, J.; Mao, Q.; Liu, Q.; Chen, H. Study on CO2 Gasification of Biochar in Molten Salts: Reactivity and Structure Evolution. *Fuel* **2019**, *254*, 115614. https://doi.org/10.1016/j.fuel.2019.06.022.
(43) Wei, J.; Guo, Q.; Gong, Y.; Ding, L.; Yu, G. Effect of Biomass Leachates on Structure Evolution and Reactivity Characteristic of Petroleum Coke Gasification. *Renewable Energy* **2020**, *155*, 111–120. https://doi.org/10.1016/j.renene.2020.03.132.